Self-Induced Uniaxial Strain in MoS_2 Monolayers with Local van der Waals-Stacked Interlayer Interactions

Kenan Zhang,[†,‡,∥] Shuhong Hu,[†] Yun Zhang,[†] Tianning Zhang,[†] Xiaohao Zhou,[†] Yan Sun,[†] Tian-Xin Li,[†] Hong Jin Fan,[§] Guozhen Shen,[*,‡] Xin Chen,[*,†] and Ning Dai[*,†,∥,⊥]

[†]National Laboratory for Infrared Physics, Shanghai Institute of Technical Physics, Chinese Academy of Sciences, Shanghai 200083, China, [‡]State Key Laboratory of Superlattices and Microstructures, Institute of Semiconductors, Chinese Academy of Sciences, Beijing 100083, China, [§]Division of Physics and Applied Physics, School of Physical and Mathematical Sciences, Nanyang Technological University, Singapore 639798, Singapore, [∥]Synergetic Innovation Center of Quantum Information and Quantum Physics, University of Science and Technology of China, Hefei, Anhui 230026, China, and [⊥]Jiangsu Collaborative Innovation Center of Photovolatic Science and Engineering, Changzhou 213164, China

ABSTRACT

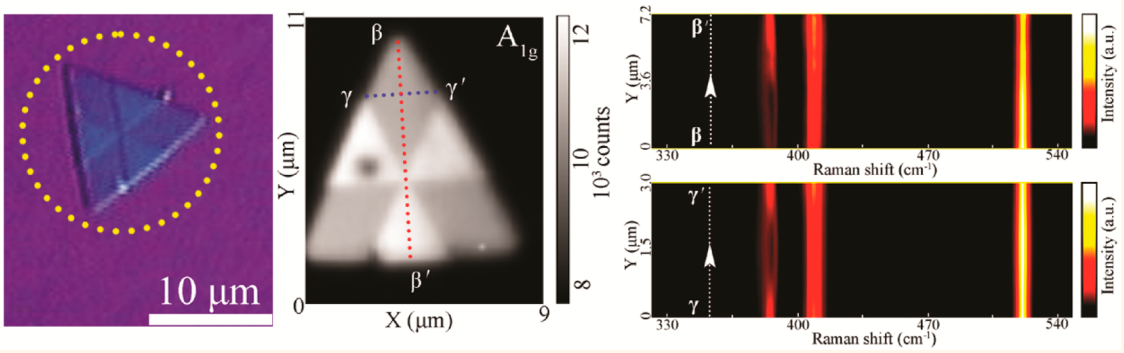

Strain engineering is an effective method to tune the properties of electrons and phonons in semiconductor materials, including two-dimensional (2D) layered materials (*e.g.*, MoS_2 or graphene). External artificial stress (ExAS) or heterostructure stacking is generally required to induce strains for modulating semiconductor bandgaps and optoelectronic functions. For layered materials, the van der Waals-stacked interlayer interaction (vdW-SI) has been considered to dominate the interlayer stacking and intralayer bonding. Here, we demonstrate self-induced uniaxial strain in the MoS_2 monolayer without the assistance of ExAS or heterostructure stacking processes. The uniaxial strain occurring in local monolayer regions is manifested by the Raman split of the in-plane vibration modes E_{2g}^1 and is essentially caused by local vdW-SI within the single layer MoS_2 due to a unique symmetric bilayer stacking. The local stacked configuration and the self-induced uniaxial strain may provide improved understanding of the fundamental interlayer interactions and alternative routes for strain engineering of layered structures.

KEYWORDS: MoS_2 · uniaxial strain · self-induced · van der Waals stacking · Raman · first-principles plane-wave calculations

Strain originating from lattice mismatch or deformation is ubiquitous and presents both promises and challenges to the electrical and optoelectronic properties of semiconductor materials. In general, for the growth of desired semiconductors with high crystalline quality, the internal strain should be minimized by controlling dislocations and grain boundaries. However, strain engineering is also useful in tuning the semiconductor bandgap and carrier transport properties and thus constitutes an important strategy for enhancing the device performance.[1−8] Strained silicon, for example, has been widely exploited in modern semiconductor microelectronic and optoelectronic technologies,[9,10] and the strained channels can enhance carrier mobility and device speed in most metal oxide−semiconductor field-effect transistors.[7,11] Recently, ExAS and heterostacking have been widely exploited to tune intralayer bonding (such as strain) and to control the exceptional behaviors of electrons and phonons in layered materials (*e.g.*, MoS_2 or graphene).[12−24]

* Address correspondence to xinchen@mail.sitp.ac.cn, gzshen@semi.ac.cn, ndai@mail.sitp.ac.cn.

Received for review November 15, 2014 and accepted February 25, 2015.

Published online February 25, 2015
10.1021/acsnano.5b00547

Internal vdW-SI is an essential driving force to dominate interlayer stacking and/or to alter intralayer bonding and, thus, has important roles in tuning the bandgap (*e.g.*, Raman modes and photoluminescence) of layered MoS_2 and graphene.[24−29] However, no uniaxial intralayer strain has been discovered in exfoliated MoS_2 layered stacking with internal vdW-SI.[25,26] As mentioned above, uniaxial strains are mostly induced in MoS_2 and graphene only by ExAS or heterostacking.[12,15,30−35] Whether a self-induced uniaxial strain can occur in layered stacking without ExAS or heterostacking is an underexplored research area. Here, we report the self-induced intralayer strain present in vapor-deposition fabricated MoS_2 monolayers with symmetrical local bilayer stacking (we refer this configuration as 1+αL). Such an uniaxial strain in the local MoS_2 monolayer without any ExAS or heterostacking is confirmed by frequency splitting of the in-plane vibration mode (E_{2g}^1) of MoS_2 and confirmed by first-principle calculation. We show that the uniaxial intralayer strain originates from finite boundary and lattice deformation due to the local internal vdW-SI that spontaneously occurs in our unique 1+αL MoS_2 structures.

RESULTS AND DISCUSSION

Our observation and demonstration began with the preparation of layered MoS_2 materials *via* a vapor−solid growth route using MoS_2 as the only source.[35,37] Figure 1 shows the optical images of these MoS_2 materials. In addition to the common monolayer (Figure 1a) and bilayer MoS_2 (Figure 1d), 1+αL MoS_2 structures are also observed (Figures 1b,c). Interestingly, three local small triangular flakes are found to be symmetrically situated atop a large triangular MoS_2 flake. Such small local stacked flakes are different from the pure monolayer and bilayer and can extend and merge (as shown in Figure 1c). These intriguing 1+αL MoS_2 structures appear to be an intermediate transition from monolayer to bilayer. Figure 1e further illustrates schematically the feature corresponding to these 1+αL MoS_2 structures.

Raman spectroscopy is a powerful and facile technique for probing phonon behaviors in layered graphene and MoS_2 and has been widely applied to identify or quantify the layer number,[25,38] strain,[12,13,39] and phonon anharmonic effects.[40] The fabricated MoS_2 monolayers are ∼0.75 nm thick, and the peak frequency difference (Δ) between the in-plane (E_{2g}^1) and out-of-plane (A_{1g}) vibrational modes is approximately 19−20 cm^{-1}.[37] Furthermore, the Raman intensities are uniformly distributed in individual triangular MoS_2 monolayers and bilayers. The fabricated MoS_2 monolayer also exhibits a direct band gap of ∼1.8 eV, which is similar to that previously reported for MoS_2 monolayers.[41,42] These basic characterizations support the feasibility of vapor−solid-growth for MoS_2 monolayer formation on SiO_2/Si substrates. In particular, the 1+αL MoS_2 structures in Figure 1, to our knowledge, have not been previously reported from either mechanical exfoliation or chemical vapor deposition.

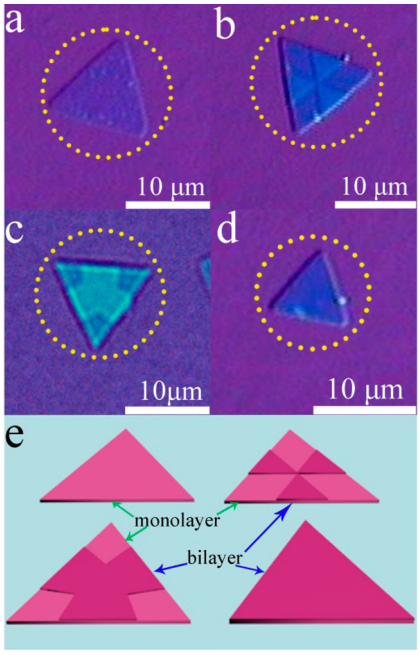

Figure 1. Optical microscopy photographs (a−d) and corresponding schematic features (e) of layered MoS_2 with different stacking structures in the yellow circles: (a) MoS_2 monolayer, (b, c) two types of 1 + αL MoS_2 structures, and (d) a bilayer.

We used the microzone Raman spectra and intensity maps of the A_{1g} mode of MoS_2 to further characterize these 1+αL MoS_2 structures. Raman spectroscopy has shown great promise for exploring strain because the strain induces changes in the crystalline symmetry and then shifts the vibrational frequency.[12,13,39] Figure 2a shows that the Raman intensity map has a contrast profile similar to that of the optical morphologies in Figure 1b. The Raman spectra in Figure 2b were taken from the regions indicated as I to VI in Figure 2a. The Raman shift at ∼520.4 cm^{-1} arises from the Si substrates. Importantly, the E_{2g}^1 mode splits to doublets with a frequency difference of ∼4−5 cm^{-1} in the indicated I, II and III regions (monolayer without stacking) but not in the IV, V and VI regions (with bilayer stacking). More obvious Raman mode splitting in the I, II and III regions were obtained by using a laser of 2 mW under a long accumulation time per acquisition, as displayed in Figure 2c (also Figure S1, Supporting Information). In addition, the AFM results shown in Figure 2d verify that the upper small triangular flake is also a monolayer (∼0.75 nm thick) and the total thickness is ∼1.45 nm. The line-scan Raman intensity maps reveal that the Raman splitting varies with scanning direction, as shown in Figure 2e and S2. As the E_{2g}^1 Raman mode splitting is closely correlated to strain,[12,13,31] we may conclude that there exists strain only in the monolayer regions but not in

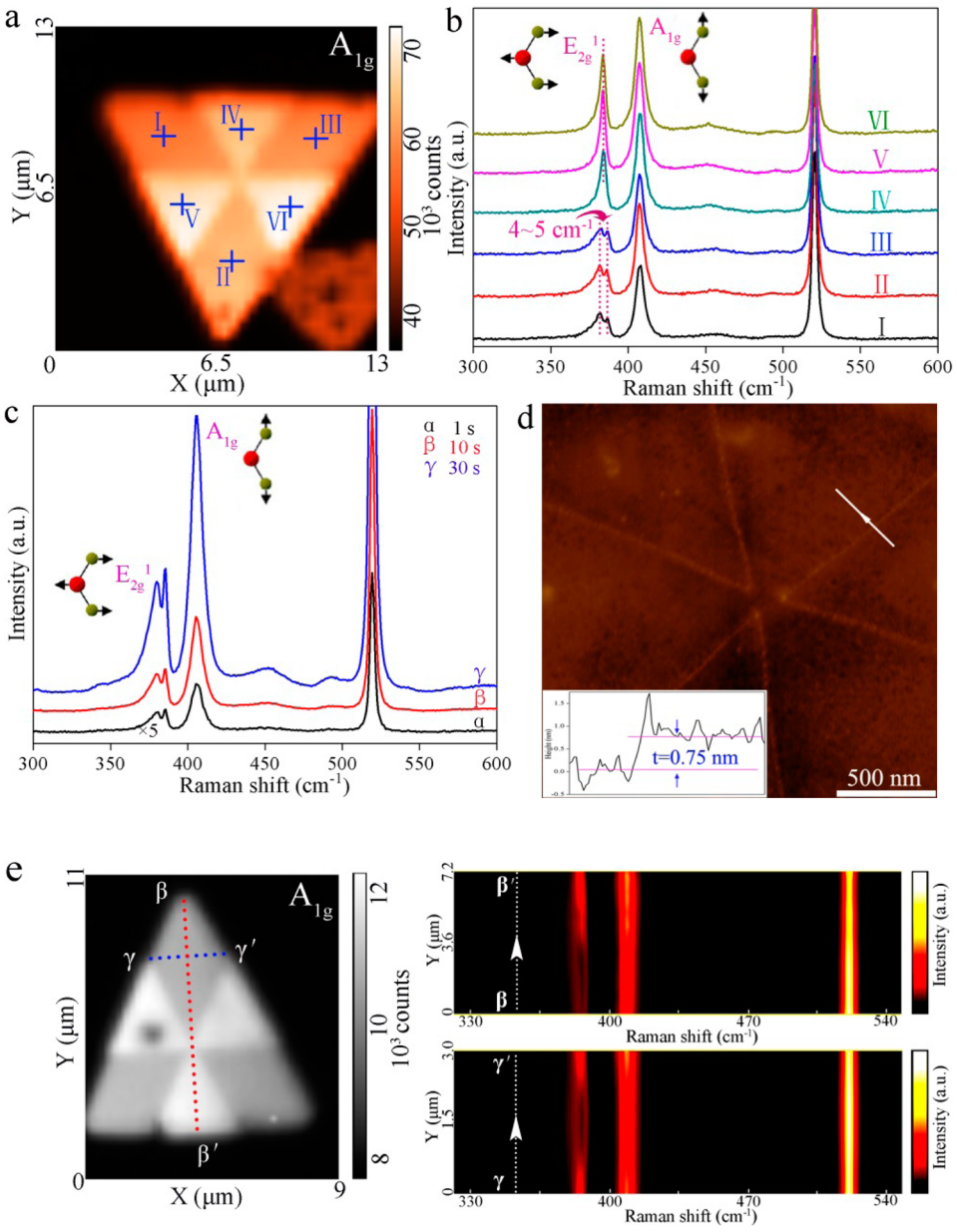

Figure 2. (a) Intensity map of the A_{1g} Raman mode for a 1+αL MoS_2 structure. (b) Raman spectra of the six regions indicated in (a). The two split E_{2g}^1 modes of MoS_2 are due to phonon degeneration in regions I, II, and III. (c) MoS_2 Raman spectra in region I with different accumulation times. (d) AFM image with a line scan (inset) of the MoS_2 flake in (a). (e) Line-scanned mapping of the Raman shifts of E_{2g}^1, A_{1g} modes of MoS_2 and of TO mode of Si. More mapping data along other directions are presented in Figure S2 (Supporting Information). Note that Raman data were obtained from randomly chosen MoS_2 triangles and different acquisition times.

the bilayer stacking regions, and the line-scan mapping data implies the strain is not uniform (*i.e.*, uniaxial). Moreover, according to previous polarized Raman results,[15,39,43] our polarized Raman data (see Figure S3, Supporting Information) also indicate that uniaxial strains exist in the local monolayer regions. To our knowledge, such self-induced (*i.e.*, without ExAS) uniaxial strain has not been discovered in mechanical exfoliated or chemical vapor deposited MoS_2 structures.[25,26,44] This result implies that the finite boundary and lattice deformation and other interlayer interactions may dominate such an uniaxial intralayer strain.[12,13,24−27]

To further verify that the mode splitting occurs only in the unique 1+αL MoS_2, Raman spectra acquired from different regions are presented and compared among different types of samples (viz., 1L, 1+αL, and 2L). Figure 3 shows the Raman intensity maps of the MoS_2 A_{1g} mode for four different types of samples. Again, it has been confirmed by AFM that the I, II, and III regions are monolayers, whereas IV, V, and VI regions are bilayers. The Raman frequency difference Δ between E_{2g}^1 and A_{1g} is ~21.9 cm^{-1}, which is similar to that for bilayer sample (2L). For single-layer sample (1L) (Figure 3a) and 2L sample (Figure 3d), the intensities

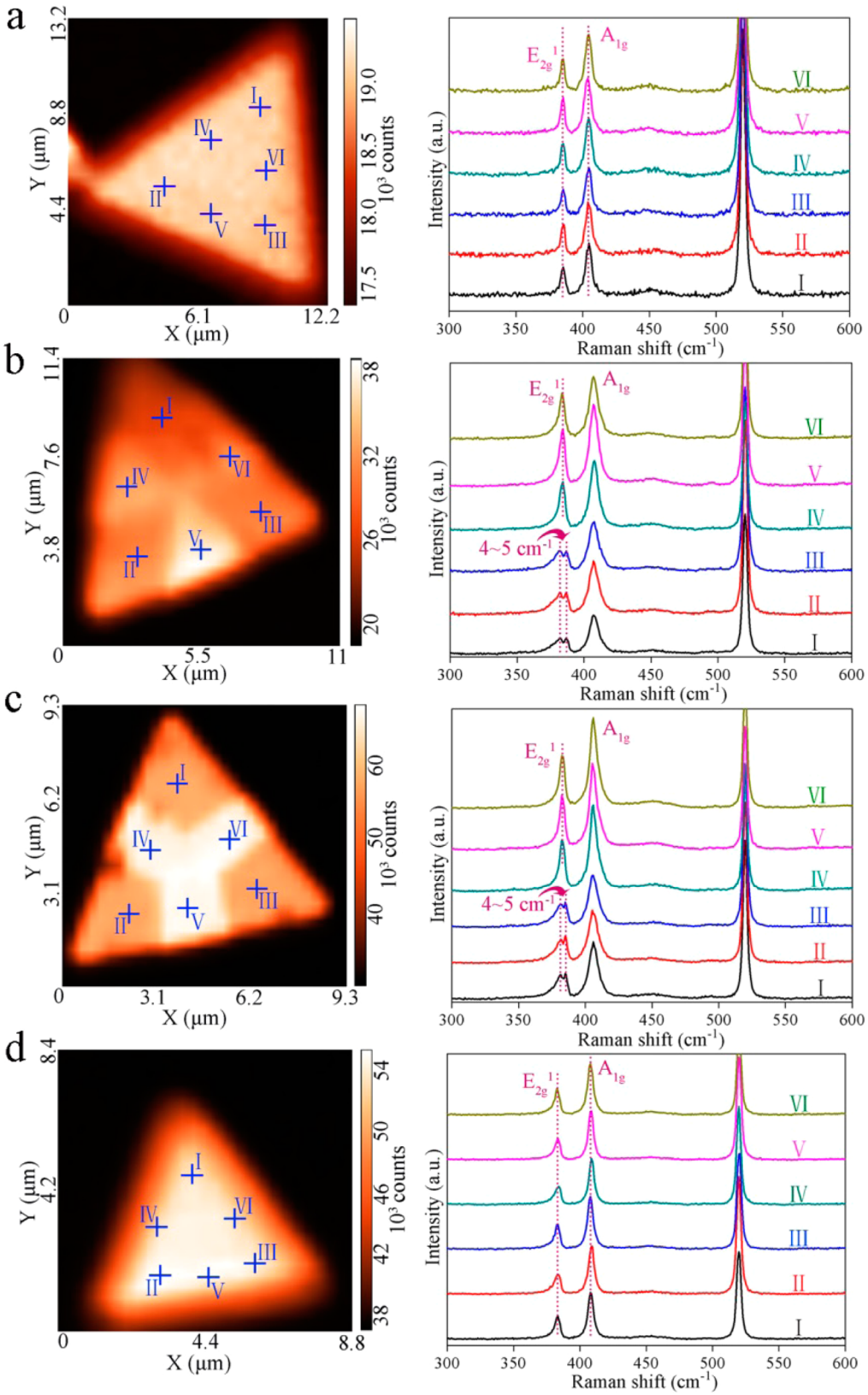

Figure 3. Raman intensity maps of the A_{1g} modes. (a) MoS_2 monolayer. (b and c) Two types of $1 + \alpha$L MoS_2 structure. (c) MoS_2 bilayer. The corresponding Raman spectra in the designated regions are presented on the right. Note that the E_{2g}^1 modes do not split in the pure monolayer and bilayer MoS_2.

are uniformly distributed. However, parts b and c of Figure 3 present obvious differences between the (I, II, III) and (IV, V, VI) regions in the Raman spectra and intensity maps. When the local stacked monolayer

was formed, the E_{2g}^1 mode splits into two subpeaks only in the I, II, and III regions but not in the IV, V, and VI regions. In the IV, V, and VI regions with three stacked local symmetrical triangular MoS_2 monolayers, the Raman signal is slightly stronger because of the increased thickness.[28] More intriguingly, this Raman mode splitting was not observed in the more common incomplete bilayers where one smaller triangle sits right atop of the underneath triangle (see Figure S4, Supporting Information). The corresponding photoluminescence (PL) intensity maps presented in Figure S5 (Supporting Information) also confirms the symmetrical local bilayer stacking structure (to be discussed below). From these results, it can be proposed that the strain occurring in the unique 1+αL MoS_2 sample stems from the symmetrical local bilayer stacking.

We next seek to determine the mechanism of E_{2g}^1 mode splitting for the 1+αL MoS_2 structure when local MoS_2 monolayers are symmetrically stacked on the bottom MoS_2 monolayer. As mentioned above, ExAS has been generally applied to induce lateral lattice deformation and consequently split or shift the E_{2g}^1 mode of layered MoS_2.[12,13,45] In our case, no ExAS is applied, so the origin should be vdW-SI in the layered MoS_2. Moreover, no splitting was observed in the E_{2g}^1 modes of layered MoS_2 in the absence of ExAS, as reported elsewhere.[46−49] One central and fascinating point here is the occurrence of uniaxial strain in such layered MoS_2 stacking with local internal vdW-SI. To confirm the strain, the first-principle plane-wave calculation was performed and showed that the lateral lattice of monolayer MoS_2 (3.189 Å) is smaller than that of bilayer MoS_2 (3.196 Å) (see Figure S6, Supporting Information). When a local monolayer is placed on top of another monolayer, the lateral lattice of the ground-monolayer region must match and coordinate with the crystalline symmetry of the MoS_2 bilayer. As a result, the stacking of two adjacent local monolayers might induce uniaxial compressive strain in the indicated I, II, and III monolayer regions, as this lattice matching leads to lattice shrinkage of the ground-monolayer regions (I, II, and III). These observations are consistent with the hypothesis that layered MoS_2 stacking can affect intralayer covalent bonds and lattice dynamics.[25,26,49] Furthermore, the vibrational properties of MoS_2 monolayer with varied strains were calculated on the basis of density-functional perturbation theory, as shown in Figure 4 (also in Figures S7 and S8, Supporting Information). The E_{2g}^1 mode splits into two modes at 384.11 and 387.70 cm^{-1} (Figure 4b) in the presence of a uniaxial compressive strain of ∼0.54%. However, the theoretical phonon dispersion curves of the MoS_2 monolayer (Figure 4c,d) indicate that the 2-D degenerate E_{2g}^1 mode at 383 cm^{-1} does not split under symmetrical biaxial compressive strain or strain-free conditions. As the calculated Raman mode splitting agrees well with the experimental values, a compressive strain of ∼0.5%

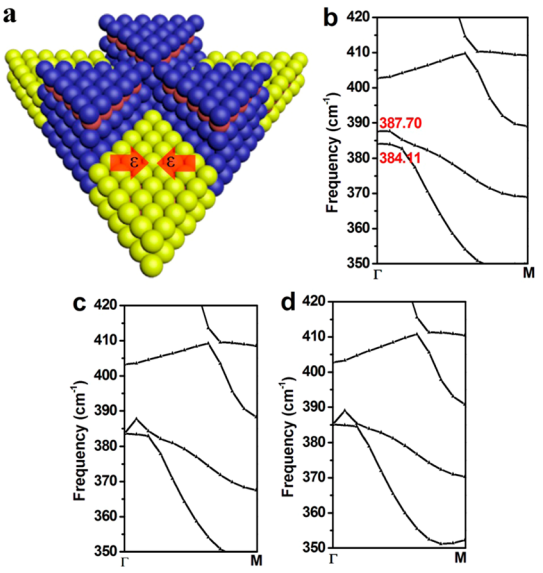

Figure 4. (a) Atomic model of a 1 + αL MoS_2 structure. The arrow indicates the uniaxial stress in the monolayer stacked region due to vdW-SI during the formation of the bilayer. Theoretical phonon dispersion of a MoS_2 monolayer: (b) under uniaxial compressive strain (∼0.54%), (c) without any strain (or free-standing), and (d) under biaxial compressive strain (∼0.54%).

is determined in these unstacked local monolayers. These results are also similar to those in the ExAS MoS_2 samples reported elsewhere.[12,13] In summary, theoretical simulation and measurements together confirm that the E_{2g}^1 splitting originates from lattice deformation (*i.e.*, uniaxial strain) induced by the local vdW-SI. Moreover, such obvious strains presented here further indicate that the finite boundary effect and other possible interlayer interactions may be another critical role.[24−28,47,49]

PL measurements were also conducted in order to study the effect of local stain to the optical bandgap. Figure 5 and Figure S9 (Supporting Information) present PL spectra and maps of the 1+αL MoS_2 structure, respectively. The intensity profile in those maps (Figure S5, Supporting Information) agrees well with the aforementioned Raman maps and optical images. Figure 5c show the PL spectra recorded from the monolayer region in the 1+αL structure (curve I) and the bilayer stacked region (curve II). The spectra are normalized in order to show the peak shift. PL of pure single-layer MoS_2 sample is also presented in curve III. One can see that the optical bandgap of the bilayer stacked region is red-shifted compared to the monolayer region in the 1+αL structure (as well as to the single layer). The PL intensity mapping shows that the monolayer regions exhibit much stronger emission than the bilayer regions. Moreover, compared with the single-layer MoS_2, the PL peak of the monolayer region in the 1+αL MoS_2 structure slightly blue-shifted. The blue-shift of the optical bandgap in the monolayer region MoS_2 might be caused by compressive strain,[45] consistent with the Raman data.

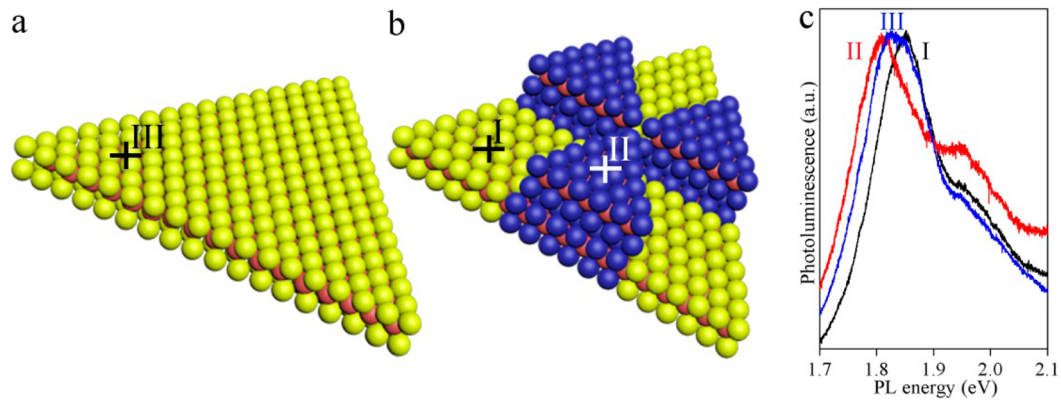

Figure 5. (a, b) Schematic of a pure MoS_2 monolayer (a) and a 1 + αL MoS_2 structure (b). (c) Normalized PL spectra recorded from the designated regions to show the peak shift.

The PL results indicate that the local vdW-SI could be an effective route to tuning of the band gap of layered MoS_2. More thorough investigations are needed to control the properties of electrons and phonons by internal vdW-SI and to understand how these layered MoS_2 stacking form during the vapor−solid growth.

CONCLUSION

We have discovered and demonstrated self-induced intralayer strain (~0.54%) in a unique 1+αL MoS_2 structure (monolayers with symmetric local bilayer stacking). The occurrence of self-induced uniaxial strain differs from the previous studies in which strains were induced by external stress or heterostructure stacking. Through comprehensive Raman photoluminescence characterization, as well as first-principles calculation, it is established that local internal vdW-SI in the symmetric bilayer stacking regions is responsible for the deformation of local intralayer bonding in the unstacked monolayer region. The discovery of self-induced intralayer strains by local vdW-SI may create alternative opportunities for strain engineering toward tunable optoelectronic functionalities.

METHODS

MoS_2 layers were fabricated on SiO_2/Si substrates by a vapor−solid growth route using the powder MoS_2 source (Sigma-Aldrich). Samples were characterized using optical microscopy (Leica DM4000M) and atomic force microscopy (AIST-NT). Raman, PL spectroscopy and the spatial mappings were conducted using a Nanofinder 30 (TII Tokyo Instruments, Inc.). All Raman spectra were measured at room temperature and were calibrated by the Raman shift of single-crystal silicon at 520.4 cm^{-1}. Raman measurements were performed using an 1800 g/mm grating to disperse the signal and generate a spectral resolution of less than 1 cm^{-1} (a 300 g/mm grating was also used for the PL mapping). PL spectra were obtained using an 1800 g/mm grating spectrometer with HORIBA LabRam HR800 Ev. We used different accumulation times per acquisition and randomly chosen MoS_2 flakes to eliminate experimental errors during Raman measurements. First-principles calculation was performed to reveal the atomic model and confirm the existence of such partially stacked monolayers. The vibrational properties were calculated according to density-functional perturbation theory.

Conflict of Interest: The authors declare no competing financial interest.

Acknowledgment. This work was funded by NSFC (61290304 and 61376016) and the National Basic Research Program of China (2012CB934301 and 2011CBA00905).

Supporting Information Available: Additional experimental details, more Raman, PL, and computational results. This material is available free of charge *via* the Internet at http://pubs.acs.org.

REFERENCES AND NOTES

1. Maiti, A. Carbon Nanotubes - Bandgap Engineering with Strain. *Nat. Mater.* **2003**, *2*, 440–442.
2. Qi, J. S.; Qian, X. F.; Qi, L.; Feng, J.; Shi, D. N.; Li, J. Strain-Engineering of Band Gaps in Piezoelectric Boron Nitride Nanoribbons. *Nano Lett.* **2012**, *12*, 1224–1228.
3. Wang, R. C.; Lin, H. Y.; Wang, C. H.; Liu, C. P. Fabrication of A Large-Area Al-Doped ZnO Nanowire Array Photosensor with Enhanced Photoresponse by Straining. *Adv. Funct. Mater.* **2012**, *22*, 3875–3881.
4. Le Ru, E. C.; Howe, P.; Jones, T. S.; Murray, R. Strain-Engineered InAs/GaAs Quantum Dots for Long-Wavelength Emission. *Phys. Rev. B* **2003**, *67*, 165303.
5. Mosca, D. H.; Vidal, F.; Etgens, V. H. Strain Engineering of the Magnetocaloric Effect in MnAs Epilayers. *Phys. Rev. Lett.* **2008**, *101*, 125503.
6. van der Zande, A.; Hone, J. Optical Materials Inspired by Strain. *Nat. Photonics* **2012**, *6*, 803–805.
7. Ourmazd, A. Nanoelectronics: The Strain of It All. *Nat. Nanotechnol.* **2008**, *3*, 381–382.
8. Jain, J. R.; Hryciw, A.; Baer, T. M.; Miller, D. A. B.; Brongersma, M. L.; Howe, R. T. A Micromachining-Based Technology for Enhancing Germanium Light Emission Via Tensile Strain. *Nat. Photonics* **2012**, *6*, 398–405.
9. Jacobsen, R. S.; Andersen, K. N.; Borel, P. I.; Fage-Pedersen, J.; Frandsen, L. H.; Hansen, O.; Kristensen, M.; Lavrinenko, A. V.; Moulin, G.; Ou, H.; et al. Strained Silicon as a New Electro-Optic Material. *Nature* **2006**, *441*, 199–202.
10. Hytch, M.; Houdellier, F.; Hue, F.; Snoeck, E. Nanoscale Holographic Interferometry for Strain Measurements in Electronic Devices. *Nature* **2008**, *453*, 1086–U1085.
11. Lee, M. L.; Fitzgerald, E. A.; Bulsara, M. T.; Currie, M. T.; Lochtefeld, A. Strained Si, SiGe, and Ge Channels for High-Mobility Metal-Oxide-Semiconductor Field-Effect Transistors. *J. Appl. Phys.* **2005**, *97*, 011101.
12. Conley, H. J.; Wang, B.; Ziegler, J. I.; Haglund, R. F., Jr.; Pantelides, S. T.; Bolotin, K. I. Bandgap Engineering of Strained Monolayer and Bilayer MoS_2. *Nano Lett.* **2013**, *13*, 3626–3630.

13. Zhu, C. R.; Wang, G.; Liu, B. L.; Marie, X.; Qiao, X. F.; Zhang, X.; Wu, X. X.; Fan, H.; Tan, P. H.; Amand, T.; et al. Strain Tuning of Optical Emission Energy and Polarization in Monolayer and Bilayer MoS_2. *Phys. Rev. B* **2013**, *88*, 121301.
14. Mohiuddin, T. M. G.; Lombardo, A.; Nair, R. R.; Bonetti, A.; Savini, G.; Jalil, R.; Bonini, N.; Basko, D. M.; Galiotis, C.; Marzari, N.; et al. Uniaxial Strain in Graphene by Raman Spectroscopy: G Peak Splitting, Gruneisen Parameters, and Sample Orientation. *Phys. Rev. B* **2009**, *79*, 205433.
15. Huang, M. Y.; Yan, H. G.; Chen, C. Y.; Song, D. H.; Heinz, T. F.; Hone, J. Phonon Softening and Crystallographic Orientation of Strained Graphene Studied by Raman Spectroscopy. *Proc. Natl. Acad. Sci. U.S.A.* **2009**, *106*, 7304–7308.
16. Okada, M.; Sawazaki, T.; Watanabe, K.; Taniguch, T.; Hibino, H.; Shinohara, H.; Kitaura, R. Direct Chemical Vapor Deposition Growth of WS_2 Atomic Layers on Hexagonal Boron Nitride. *ACS Nano* **2014**, *8*, 8273–8277.
17. Shi, Y.; Zhou, W.; Lu, A. Y.; Fang, W.; Lee, Y. H.; Hsu, A. L.; Kim, S. M.; Kim, K. K.; Yang, H. Y.; Li, L. J.; et al. van der Waals Epitaxy of MoS_2 Layers Using Graphene As Growth Templates. *Nano Lett.* **2012**, *12*, 2784–2791.
18. Cheng, R.; Li, D.; Zhou, H.; Wang, C.; Yin, A.; Jiang, S.; Liu, Y.; Chen, Y.; Huang, Y.; Duan, X. F. Electroluminescence and Photocurrent Generation from Atomically Sharp WSe_2/MoS_2 Heterojunction p-n Diodes. *Nano Lett.* **2014**, *14*, 5590–5597.
19. Yu, W. J.; Li, Z.; Zhou, H. L.; Chen, Y.; Wang, Y.; Huang, Y.; Duan, X. F. Vertically Stacked Multi-Heterostructures of Layered Materials for Logic Transistors and Complementary Inverters. *Nat. Mater.* **2013**, *12*, 246–252.
20. Yu, W. J.; Liu, Y.; Zhou, H. L.; Yin, A. X.; Li, Z.; Huang, Y.; Duan, X. F. Highly Efficient Gate-Tunable Photocurrent Generation in Vertical Heterostructures of Layered Materials. *Nat. Nanotechnol.* **2013**, *8*, 952–958.
21. He, K.; Poole, C.; Mak, K. F.; Shan, J. Experimental Demonstration of Continuous Electronic Structure Tuning Via Strain in Atomically Thin MoS_2. *Nano Lett.* **2013**, *13*, 2931–2936.
22. Hannah, D. C.; Yang, J. H.; Podsiadlo, P.; Chan, M. K. Y.; Demortiere, A.; Gosztola, D. J.; Prakapenka, V. B.; Schatz, G. C.; Kortshagen, U.; Schaller, R. D. On the Origin of Photoluminescence in Silicon Nanocrystals: Pressure-Dependent Structural and Optical Studies. *Nano Lett.* **2012**, *12*, 4200–4205.
23. Brunner, K. Si/Ge Nanostructures. *Rep. Prog. Phys.* **2002**, *65*, 27–72.
24. Pereira, V. M.; Neto, A. H. C.; Peres, N. M. R. Tight-Binding Approach to Uniaxial Strain in Graphene. *Phys. Rev. B* **2009**, *80*, 045401.
25. Lee, C.; Yan, H.; Brus, L. E.; Heinz, T. F.; Hone, J.; Ryu, S. Anomalous Lattice Vibrations of Single- and Few-Layer MoS_2. *ACS Nano* **2010**, *4*, 2695–2700.
26. Li, H.; Zhang, Q.; Yap, C. C. R.; Tay, B. K.; Edwin, T. H. T.; Olivier, A.; Baillargeat, D. From Bulk to Monolayer MoS_2: Evolution of Raman Scattering. *Adv. Funct. Mater.* **2012**, *22*, 1385–1390.
27. Ghosh, P. N.; Maiti, C. R. Interlayer Force and Davydov Splitting in 2h-MoS_2. *Phys. Rev. B* **1983**, *28*, 2237–2239.
28. Splendiani, A.; Sun, L.; Zhang, Y.; Li, T.; Kim, J.; Chim, C. Y.; Galli, G.; Wang, F. Emerging Photoluminescence in Monolayer MoS_2. *Nano Lett.* **2010**, *10*, 1271–1275.
29. Lee, J. E.; Ahn, G.; Shim, J.; Lee, Y. S.; Ryu, S. Optical Separation of Mechanical Strain from Charge Doping in Graphene. *Nat. Commun.* **2012**, *3*, 1024.
30. Lee, C.; Wei, X. D.; Kysar, J. W.; Hone, J. Measurement of the Elastic Properties and Intrinsic Strength of Monolayer Graphene. *Science* **2008**, *321*, 385–388.
31. Cooper, R. C.; Lee, C.; Marianetti, C. A.; Wei, X.; Hone, J.; Kysar, J. W. Nonlinear Elastic Behavior of Two-Dimensional Molybdenum Disulfide. *Phys. Rev. B* **2013**, *87*, 035423.
32. Feng, J.; Qian, X. F.; Huang, C. W.; Li, J. Strain-Engineered Artificial Atom As A Broad-Spectrum Solar Energy Funnel. *Nat. Photonics* **2012**, *6*, 865–871.
33. Guinea, F.; Katsnelson, M. I.; Geim, A. K. Energy Gaps and A Zero-Field Quantum Hall Effect in Graphene by Strain Engineering. *Nat. Phys.* **2010**, *6*, 30–33.
34. Zhang, D. B.; Seifert, G.; Chang, K. Strain-Induced Pseudomagnetic Fields in Twisted Graphene Nanoribbons. *Phys. Rev. Lett.* **2014**, *112*, 096805.
35. Nayak, A. P.; Bhattacharyya, S.; Zhu, J.; Liu, J.; Wu, X.; Pandey, T.; Jin, C.; Singh, A. K.; Akinwande, D.; Lin, J. F. Pressure-Induced Semiconducting to Metallic Transition in Multilayered Molybdenum Disulphide. *Nat. Commun.* **2014**, *5*, 3731.
36. Wu, S. F.; Huang, C. M.; Aivazian, G.; Ross, J. S.; Cobden, D. H.; Xu, X. D. Vapor-Solid Growth of High Optical Quality MoS_2 Monolayers with Near-Unity Valley Polarization. *ACS Nano* **2013**, *7*, 2768–2772.
37. Zhang, K. N.; Zhang, Y.; Zhang, T. N.; Dong, W. J.; Wei, T. X.; Sun, Y.; Chen, X.; Shen, G. Z.; Dai, N. Vertically Coupling ZnO Nanorods on MoS_2 Monolayers with Enhanced Raman and Photoluminescence Emission. *Nano Res.* **2014**, 10.1007/s12274-014-0557-1.
38. Ferrari, A. C.; Meyer, J. C.; Scardaci, V.; Casiraghi, C.; Lazzeri, M.; Mauri, F.; Piscanec, S.; Jiang, D.; Novoselov, K. S.; Roth, S.; et al. Raman Spectrum of Graphene and Graphene Layers. *Phys. Rev. Lett.* **2006**, *97*, 187401.
39. Yoon, D.; Son, Y. W.; Cheong, H. Strain-Dependent Splitting of the Double-Resonance Raman Scattering Band in Graphene. *Phys. Rev. Lett.* **2011**, *106*, 155502.
40. Bonini, N.; Lazzeri, M.; Marzari, N.; Mauri, F. Phonon Anharmonicities in Graphite and Graphene. *Phys. Rev. Lett.* **2007**, *99*, 176802.
41. Ling, X.; Lee, Y. H.; Lin, Y. X.; Fang, W. J.; Yu, L. L.; Dresselhaus, M. S.; Kong, J. Role of the Seeding Promoter in MoS_2 Growth by Chemical Vapor Deposition. *Nano Lett.* **2014**, *14*, 464–472.
42. van der Zande, A. M.; Huang, P. Y.; Chenet, D. A.; Berkelbach, T. C.; You, Y. M.; Lee, G. H.; Heinz, T. F.; Reichman, D. R.; Muller, D. A.; Hone, J. C. Grains and Grain Boundaries in Highly Crystalline Monolayer Molybdenum Disulphide. *Nat. Mater.* **2013**, *12*, 554–561.
43. Wang, Y. L.; Cong, C. X.; Qiu, C. Y.; Yu, T. Raman Spectroscopy Study of Lattice Vibration and Crystallographic Orientation of Monolayer MoS_2 Under Uniaxial Strain. *Small* **2013**, *9*, 2857–2861.
44. Liu, Z.; Amani, M.; Najmaei, S.; Xu, Q.; Zou, X. L.; Zhou, W.; Yu, T.; Qiu, C. Y.; Birdwell, A. G.; Crowne, F. J.; et al. Strain and Structure Heterogeneity in MoS_2 Atomic Layers Grown by Chemical Vapour Deposition. *Nat. Commun.* **2014**, *5*, 5246.
45. Hui, Y. Y.; Liu, X. F.; Jie, W. J.; Chan, N. Y.; Hao, J. H.; Hsu, Y. T.; Li, L. J.; Guo, W. L.; Lau, S. P. Exceptional Tunability of Band Energy in A Compressively Strained Trilayer MoS_2 Sheet. *ACS Nano* **2013**, *7*, 7126–7131.
46. Najmaei, S.; Liu, Z.; Zhou, W.; Zou, X.; Shi, G.; Lei, S.; Yakobson, B. I.; Idrobo, J. C.; Ajayan, P. M.; Lou, J. Vapour Phase Growth and Grain Boundary Structure of Molybdenum Disulphide Atomic Layers. *Nat. Mater.* **2013**, *12*, 754–759.
47. Liu, K.; Zhang, L.; Cao, T.; Jin, C.; Qiu, D.; Zhou, Q.; Zettl, A.; Yang, P.; Louie, S. G.; Wang, F. Evolution of Interlayer Coupling in Twisted MoS_2 Bilayers. *Nat. Commun.* **2014**, *5*, 4966.
48. Liu, Y.; Ghosh, R.; Wu, D.; Ismach, A.; Ruoff, R.; Lai, K. Mesoscale Imperfections in MoS_2 Atomic Layers Grown by A Vapor Transport Technique. *Nano Lett.* **2014**, *14*, 4682–4686.
49. Zhang, X.; Han, W. P.; Wu, J. B.; Milana, S.; Lu, Y.; Li, Q. Q.; Ferrari, A. C.; Tan, P. H. Raman Spectroscopy of Shear and Layer Breathing Modes in Multilayer MoS_2. *Phys. Rev. B* **2013**, *87*, 115413.